Corrected 9 July 2020. See full text.

RESEARCH ARTICLE SUMMARY

ORGANOIDS

Human CNS barrier-forming organoids with cerebrospinal fluid production

Laura Pellegrini, Claudia Bonfio, Jessica Chadwick, Farida Begum, Mark Skehel, Madeline A. Lancaster*

INTRODUCTION: The choroid plexus is a secretory epithelial tissue of the central nervous system (CNS) responsible for cerebrospinal fluid (CSF) production and functions as a barrier that regulates entry of compounds and nutrients into the brain. The CSF plays key roles in the delivery of nutrients to the brain, circulation of instructive signaling molecules, and clearance of toxic by-products such as protein aggregates.

RATIONALE: Current understanding of the choroid plexus and CSF has primarily come from animal models or CSF collected from human volunteers. These have yielded insight into general CSF composition, but the specific cellular and tissue sources of various secreted proteins have remained elusive. There is also limited understanding of the development of the choroid plexus in humans and of the relative changes in CSF composition over time. All of these deficiencies in our understanding come from a lack of experimental access to the human choroid plexus. Although several previous studies have successfully generated cells with a choroid plexus identity from human pluripotent stem cells, none have been able to recapitulate the morphology, maturation, and function of the choroid plexus, and currently, no in vitro model exists for authentic human CSF. Knowledge of the processes that regulate choroid plexus development and CSF composition could provide better strategies to manipulate and therapeutically target this vital brain tissue.

RESULTS: To study the development and function of the human choroid plexus, we developed a pluripotent stem cell–derived organoid model. Choroid plexus organoids recapitulate key morphological and functional features of human choroid plexus. First, organoids form a tight barrier that selectively regulates the entry of small molecules such as dopamine. We demonstrate that organoids can qualitatively and quantitatively predict the permeability of new drugs, and we take advantage of this system to reveal a potential toxic accumulation of BIA 10-2474, a drug that caused severe neurotoxicity only in humans and not in animal models tested. Second, choroid plexus organoids secrete a CSF-like fluid containing proteins and known biomarkers within self-contained compartments. We examine changes in secretion of CSF proteins over time and identify distinct cell types within the epithelium that contribute to dynamic changes in CSF composition. We find that these cell types can be traced to rather obscure descriptions in the literature of "dark" and "light" cells, and we demonstrate that these cells exhibit opposing features related to mitochondria and cilia. We also uncover a previously unidentified cell type in the choroid plexus: myoepithelial cells. These interacting subpopulations exhibit distinct secretory roles in CSF production and reveal previously uncharacterized human-specific secreted proteins that may play important roles in human brain development.

ON OUR WEBSITE

Read the full article at https://dx.doi.org/10.1126/science.aaz5626

CONCLUSION: Human choroid plexus organoids provide an easily tractable system to study the key functions of this organ: CSF secretion and selective transport into the CNS. As such, they can predict CNS permeability of new compounds to aid in the development of neurologically relevant therapeutics. They also provide a source of more authentic CSF and can be used to understand development of this key organ in brain development and homeostasis. ■

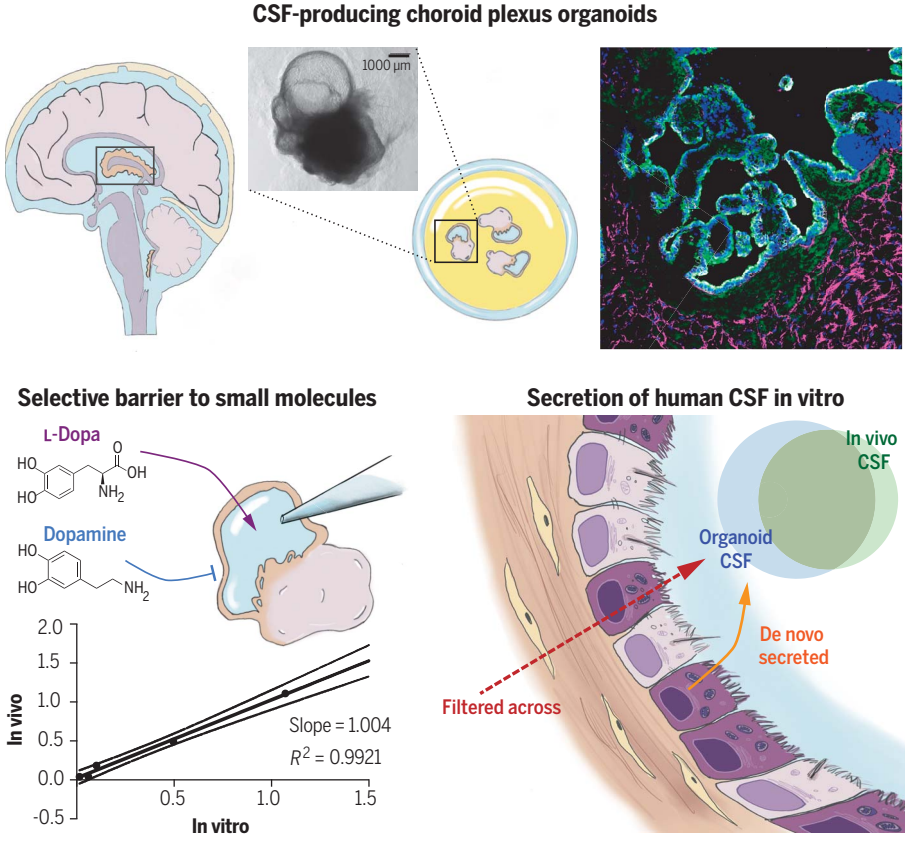

CSF-producing choroid plexus organoids predict CNS permeability of drugs. Choroid plexus organoids develop highly intricate folded tissue morphology (section stained for choroid plexus markers shown at top right) similar to choroid plexus tissue in vivo (top left) and, later, self-contained fluid-filled compartments containing a CSF-like fluid (top middle) that is separate from media. (Bottom left) Choroid plexus organoids accurately predict the permeability of small molecules such as dopamine and levodopa (L-dopa) and quantitatively predict the permeability of a range of therapeutic molecules. The graph shows the correlation between permeability in vivo and in vitro for the drugs tested. R^2, coefficient of determination. (Bottom right) Single-cell RNA sequencing reveals newly identified epithelial subtypes (colored dark and light) that participate in filtration and specialized secretion of CSF proteins. The Venn diagram shows overlap between proteins detected in CSF in vivo and in the organoid.

MRC Laboratory of Molecular Biology, Francis Crick Avenue, Cambridge CB2 0QH, UK.
*Corresponding author. Email: mlancast@mrc-lmb.cam.ac.uk
Cite this article as L. Pellegrini *et al.*, *Science* **369**, eaaz5626 (2020). DOI: 10.1126/science.aaz5626

Corrected 9 July 2020. See full text.

RESEARCH ARTICLE

ORGANOIDS

Human CNS barrier-forming organoids with cerebrospinal fluid production

Laura Pellegrini, Claudia Bonfio, Jessica Chadwick, Farida Begum, Mark Skehel, Madeline A. Lancaster*

Cerebrospinal fluid (CSF) is a vital liquid, providing nutrients and signaling molecules and clearing out toxic by-products from the brain. The CSF is produced by the choroid plexus (ChP), a protective epithelial barrier that also prevents free entry of toxic molecules or drugs from the blood. Here, we establish human ChP organoids with a selective barrier and CSF-like fluid secretion in self-contained compartments. We show that this in vitro barrier exhibits the same selectivity to small molecules as the ChP in vivo and that ChP-CSF organoids can predict central nervous system (CNS) permeability of new compounds. The transcriptomic and proteomic signatures of ChP-CSF organoids reveal a high degree of similarity to the ChP in vivo. Finally, the intersection of single-cell transcriptomics and proteomic analysis uncovers key human CSF components produced by previously unidentified specialized epithelial subtypes.

The polarized, secretory epithelium of the choroid plexus (ChP) plays a central role in brain development and function by actively secreting the cerebrospinal fluid (CSF) and forming the blood-CSF barrier (B-CSF-B) (*1*). The CSF is a colorless fluid that is rich in nutrients, hormones, and signaling molecules that are vital for brain function (*2*–*4*). The B-CSF-B, similar to the blood-brain barrier (BBB), prevents toxic substances in the circulation from reaching the brain (*5*); it directly contacts the CSF rather than the brain parenchyma and is formed by the ChP epithelial monolayer (*5*, *6*). The BBB and B-CSF-B together make up the central nervous system (CNS) barrier and prevent entry of most therapeutic molecules into the brain.

Because the ChP lies deep within the brain, study of ChP function has represented a challenge. In particular, the cellular makeup of the ChP is not well defined. Although there are reports of ChP epithelial subtypes referred to as "dark" and "light" cells owing to their observed density in transmission electron microscopy (*7*), whether heterogeneous subtypes of epithelial cells exist in this tissue is still unclear. Because the ChP is surrounded by brain tissue and vasculature, it has not been possible to examine the ChP in isolation and understand which of the many roles of the ChP are carried out by which cells and which CSF factors are filtered from the blood versus made de novo by the ChP.

Cerebral organoids can model the human developing brain with notable fidelity (*8*–*10*). Recent work by Sakaguchi *et al*. demonstrated the ability to generate dorsal identities, including the ChP and hippocampus (*11*). However, none of the key functions of the ChP (barrier formation or CSF production) were demonstrated. Thus, we are still in need of an authentic in vitro model of the ChP (*12*). To better understand the development of the human ChP and B-CSF-B and the synthesis of CSF, we have established ChP organoids. ChP organoids reliably and reproducibly develop ChP epithelium with polarized cells that actively secrete a colorless fluid with properties closely resembling the CSF. The CSF-like fluid is enclosed and isolated from the surrounding media, modeling two fundamental properties of the ChP: CSF secretion and barrier formation. With this model, we are now able to elucidate which components of the CSF are specifically generated by the ChP and assign distinct roles to newly identified ChP epithelial subtypes.

Generation of ChP organoids from human pluripotent stem cells

Cerebral organoids are characterized by self-organization of complex tissue architectures similar to the developing mammalian brain (*8*–*10*). Recent protocols describe predominantly forebrain, telencephalic identities (*13*, *14*) that also include ChP epithelium (fig. S1A) (*9*, *13*). To develop an in vitro model of human ChP with accurate architecture and function, we established a protocol based on the cerebral organoid method. In vitro derivation of ChP cells using the dorsalizing factor Bmp4, critical for the development of ChP epithelial cells both alone (*15*) and in combination with the Wnt-activator molecule CHIR (*11*), has been reported before. To promote ChP fate in cerebral organoids, Bmp4 and CHIR were given as a pulse (Fig. 1A and fig. S1B). At day 14, undirected telencephalic organoids developed large, rounded neuroepithelial lobes, whereas Bmp4 and CHIR–treated organoids generated elongated neuroepithelial tissues (fig. S1C), consistent with the progressive elongation of the ChP from the neuroepithelium of the dorsal midline in vivo (*1*, *16*, *17*). ChP organoids appeared almost entirely enriched in cuboidal epithelium, in contrast to forebrain organoids (Fig. 1, B and C). A notable feature of ChP organoids was the later development of fluid-filled compartments or "cysts" containing a colorless liquid, rarely present in untreated organoids (Fig. 1B and fig. S1D). Comparison of histological sections of ChP organoids with human and mouse embryonic ChP showed a resemblance in complexity and organization between the human and the organoid samples (Fig. 1D).

In vivo, ChP epithelium starts as a pseudostratified epithelium, followed by an intermediate columnar stage, and maturing into a highly folded cuboidal epithelium (*1*, *17*, *18*). ChP organoids similarly developed a pseudostratified neuroepithelium with transthyretin (TTR)–positive areas by day 28 (fig. S1E). By approximately day 40, ChP organoids displayed more columnar and cuboidal epithelia, increasingly enriched in TTR and the cell-cell junction marker ZO1, with only sparse neuroepithelial SOX2-positive cells (Fig. 1E and fig. S1E). Cells surrounding fluid-filled compartments also stained positive for TTR and displayed polarized apical staining for AQP1 (fig. S1, F and G). Quantification of TTR-positive regions showed enrichment in ChP organoids (Fig. 1F). We detected high levels of CLIC6, a highly specific marker of the ChP (*19*) (Fig. 1, G and H), as well as a number of other ChP-related proteins (PLEC, APOE, PLTP, IGFBP7, CA2) with lower levels of the telencephalic marker Foxg1 and other neuronal markers (DCX, GAP43) (Fig. 1H and fig. S3A). Cortical Tbr2 intermediate progenitors and HuC/D neurons were also largely reduced in early ChP organoids and almost completely absent in mature ChP organoids compared with controls (fig. S3B). Together, these data demonstrate a reliable and reproducible generation of ChP tissue in vitro, as well as fluid-filled compartments, from different lines of human pluripotent stem cells and with two different seeding methods (Fig. 1F and fig. S2, A to F).

ChP organoids develop epithelial and stromal components and recapitulate the in vivo human transcriptomic signature

To further investigate the identity of ChP organoids, we performed single-cell RNA-sequencing (scRNA-seq), sampling two organoids from three separate batches of ChP organoids and two telencephalic organoids as a control (Fig. 1, I and J). Combined analysis revealed that cells from different ChP organoid batches were intermingled and largely separate from those of telencephalic organoids (Fig. 1I), suggesting reproducibility across batches. Furthermore, although telencephalic organoid cells expressed

MRC Laboratory of Molecular Biology, Francis Crick Avenue, Cambridge CB2 0QH, UK.
*Corresponding author. Email: mlancast@mrc-lmb.cam.ac.uk

Corrected 9 July 2020. See full text.

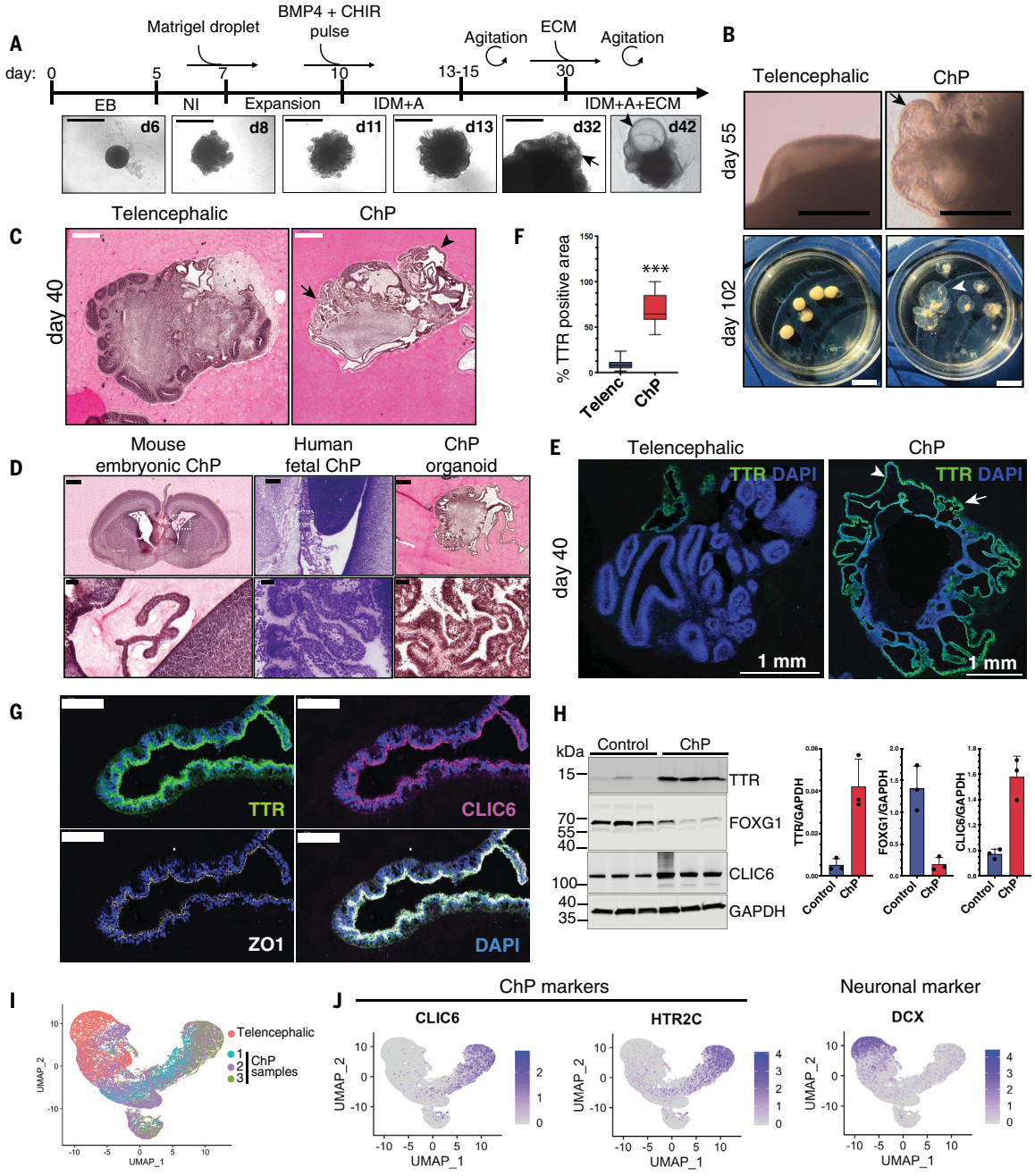

Fig. 1. Generation of human ChP organoids with self-contained fluid-filled compartments. (**A**) Protocol timeline with images of H9 round-seeded ChP organoids over time. The arrow indicates emerging ChP epithelium and the arrowhead the later fluid-filled compartment. The notation "d" indicates "day." Scale bars, 1000 μm. EB, embryoid body; NI, neural induction; IDM+A, improved differentiation media+vitamin A; IDM+A+ECM, IDM+A+extracellular matrix (Matrigel). (**B**) Comparison of H1 ChP and telencephalic organoids (day 55, scale bars 1 mm; and day 102, scale bars, 1 cm). The arrow indicates ChP epithelium, and the arrowhead points to a fluid-filled cavity. (**C**) Hematoxylin and eosin (H&E)–stained sections of H1 telencephalic and ChP organoids (day 40). The arrow indicates convoluted ChP epithelium, and the arrowhead points to a fluid-filled cavity. Scale bars, 500 μm. (**D**) Histological sections of E18.5 mouse embryonic brain (H&E stained), human fetal ChP at 15 postconception weeks [Nissl stained, from BrainSpan Atlas of the Developing Human Brain (*45*)], and H1 human ChP organoid at day 40 (H&E stained). The bottom images are magnified views of the areas indicated by the dotted rectangles in the top images. Scale bars, 500 μm (top) and 50 μm (magnified views). (**E**) Representative confocal images of H1 telencephalic and ChP organoids at day 40 stained for TTR and nuclei [4′,6-diamidino-2-phenylindole (DAPI), blue]. The arrow indicates convoluted TTR-positive ChP epithelium, and the arrowhead points to ChP epithelium surrounding a fluid-filled cavity. (**F**) Quantification of the percentage of TTR-positive area over total organoid area in $n = 4$ independent H9 batches (three or four organoids per batch, days 30, 40, and 48). Error bars represent SEM. ***$P < 0.00001$, Mann-Whitney test. Telenc, telencephalic. (**G**) Representative confocal images of ChP epithelium from H1 organoid (day 40) stained for TTR, CLIC6, ZO1, and DAPI. Scale bars, 50 μm. (**H**) Immunoblots from telencephalic control and ChP organoids probed for TTR, FOXG1, CLIC6, and loading control glyceraldehyde phosphate dehydrogenase (GAPDH). Quantification of immunoblots shows band intensity normalized for GAPDH ($n = 3$ independent H9 batches collected at days 75, 73, and 68, in separate lanes). Error bars represent SEM. (**I**) Uniform manifold approximation and projection (UMAP) dimensional reduction plot of the combined samples (telencephalic organoids and three ChP organoids), showing overlap among ChP organoid cells. (**J**) Feature plots showing enrichment of ChP markers CLIC6 and HTR2C in ChP cells and of neuronal marker DCX in telencephalic organoid cells.

neuronal markers, such as DCX, ChP cells expressed ChP markers, such as CLIC6 and HTR2C (*20*) (Fig. 1J).

Cluster analysis revealed five major cell types: two major telencephalic clusters consisting of neural progenitors and neurons and three major ChP clusters. Further examination of marker genes revealed an immature ChP cluster expressing early regulatory factors involved in ChP development, including MSX1, OTX2, and R-spondin 3 (RSPO3). This cluster also expressed the progenitor marker PAX6, which was also expressed in the neural progenitor cluster of telencephalic organoids (Fig. 2, A and B) owing to their common developmental origin. The third cluster of the ChP organoids expressed numerous mesenchymal markers, including the extracellular matrix component COL1A1 (Fig. 2A), DCN, LUM, and DLK1 (Fig. 2B). These markers allowed us to assign three major identities to ChP organoids: immature ChP/hem, mature ChP epithelium, and ChP stroma (Fig. 2C). Further analysis also revealed a consistent and progressive enrichment over time in the mature ChP cluster (Fig. 2, D and E). Immunostaining highlighted both stromal and epithelial cells (Fig. 2F and fig. S3C), and examination of regional ChP markers (*4*, *20*) revealed the ChP organoids to be of lateral ventricle identity rather than third or fourth ventricle (Fig. 2G), consistent with their telencephalic origin.

Comparison with a published scRNA-seq dataset of developing human brain (*21*) revealed a high correlation between organoid and in vivo ChP clusters and between organoid and in vivo stromal clusters (Fig. 2, H and I). Further comparison to both human in vivo ChP and developing mouse ChP from scRNA-seq of mouse embryos (*22*) revealed a higher correlation with human ChP than with mouse (Fig. 2J and fig. S3D). Overall, these data demonstrate that in vitro–derived ChP organoids closely recapitulate the cell composition and transcriptomic signature of the human ChP in vivo.

ChP organoids form a tight barrier and recapitulate in vivo CNS permeability to small molecules

To test the functional role of ChP organoids in the formation of a selective barrier, we first assessed expression of tight junction markers such as claudins and occludin (OCLN). scRNA-seq revealed the presence of several of the claudins (CLDN1, CLDN3, CLDN5) (Fig. 3A) as well as other tight junction components OCLN, ZO1 (TJP1), ZO2 (TJP2), and PDZ proteins PATJ (INADL) and MPDZ (Fig. 3B). We observed apical localization of CLDN1, CLDN3, CLDN4, and CLDN5 in the ChP epithelium (Fig. 3C). Low levels of CLDN2 were also observed in ChP organoid epithelium (fig. S4) as well as the presence of OCLN (fig. S4). Electron micrographs also revealed tight junctions, as well as primary cilia, extensive microvilli, multivesicular bodies, and numerous extracellular vesicles (Fig. 3D). We directly assessed barrier function by examining the entry of fluorescently labeled dextrans of varying molecular weights, which were completely excluded from the organoid (Fig. 3, E and F).

To test for more selective permeability, we applied therapeutically relevant small molecules and assayed their permeability by nuclear magnetic resonance (NMR) analysis (Fig. 4A and table S1). As a proof of principle, we tested dopamine (dopa) and its precursor, levodopa (L-dopa), because these are similar molecules with very different permeability in vivo. Dopa does not enter the brain in vivo, whereas L-dopa is actively transported into the CSF via the LAT-1 transporter (*23*, *24*). We incubated the organoids with dopa and L-dopa in the presence of carbidopa, a small molecule that prevents conversion of L-dopa into dopa (*25*). After 2 hours, both compounds were detectable in the media, but only L-dopa was detectable in the organoid internal fluid, demonstrating that our model exhibited the same selectivity in vitro as in vivo (Fig. 4B and fig. S5). LAT-1 was expressed on the ChP organoid epithelium (Fig. 4, C and D), explaining the proper transport of L-dopa in our assay. We also detected expression of efflux pump P-glycoprotein 1 (Pgp/MDR1) throughout the apicobasal axis (Fig. 4C). Pgp localization in ChP has been somewhat controversial (*26*); however, it is reported to have a role in pumping molecules from the CSF to the blood (*26*, *27*). These findings would suggest that the Pgp is expressed in the human ChP. Additionally, ChP efflux transporters MRP1 and MRP4 (*26*, *28*) were localized on ChP organoid epithelium (Fig. 4, D and E). These results suggest that ChP organoids express transporters that are critical for the correct function of the B-CSF-B in human brain.

We next tested whether the system could quantitatively predict drug permeability. We tested bupropionyl, an antidepressant known to readily cross the BBB (*29*), and two chemotherapeutic compounds, methotrexate and vincristine, which poorly cross the BBB owing to the actions of efflux transporters MRP1/4 and Pgp, respectively (*30*, *31*). As expected, bupropionyl was readily detectable in the organoid internal fluid after 2 hours, whereas methotrexate and vincristine were completely excluded from the internal fluid (Fig. 4F and figs. S6 and S7). We found high correlation between in vitro fluid/media ratios and the in vivo CSF/plasma ratios reported in the literature for the same drugs [coefficient of determination (R^2) = 0.9921] (Fig. 4G and table S2). The values corresponded well (as indicated by a slope of 1.004), indicating that this in vitro system can qualitatively and quantitatively recapitulate the permeability of drugs reported in vivo.

To test whether ChP organoids could predict CNS permeability of new drugs, we turned to Sephin 1, an inhibitor of the regulatory subunit PPP1R15A of protein phosphatase 1 (*32*). Clinical trials for this promising candidate have recently begun, but data for this molecule in humans are not yet available. Sephin 1 was detectable in organoid internal fluid, indicating that this compound could also cross the human CNS barrier (Fig. 4H and fig. S6). Notably, however, the permeability in the human organoid model was much lower than that described in mice (Fig. 4G). This may indicate potential species-related differences in the CNS permeability of this compound, though an in vitro difference cannot be excluded.

Issues related to the pharmacokinetic profile of drugs account for most clinical trial failures (*33*). One example involved the compound BIA 10-2474, a fatty acid amide hydrolase inhibitor that was in development for treatment of chronic pain and multiple sclerosis (*34*, *35*). Phase 1 clinical trials were halted when trial participants exhibited severe neurotoxicity, with one fatality (*34*, *36*). Investigations hypothesized toxic drug accumulation in the brain that was not evident in any animal model tested (*34*, *36*, *37*). However, the exact cause remains unknown. We compared the pharmacokinetic profile of BIA 10-2474 with that of a safe compound, bupropionyl, which crosses the barrier but has not been shown to accumulate. Similar to bupropionyl, BIA 10-2474 crossed the ChP epithelial barrier after a 2-hour incubation (Fig. 4I and fig. S8). However, compared with bupropionyl, which stabilized to baseline levels after 24 hours, BIA 10-2474 continued to accumulate in the organoid fluid (Fig. 4J). These data are consistent with the theory that BIA 10-2474 accumulated in the brains of the trial participants.

ChP organoids secrete a CSF-like fluid highly similar to in vivo CSF

The other key function of the ChP is production of CSF. We detected expression of transporters involved in CSF secretion, including the water channel aquaporin 1 (AQP1) and the key enzymes for generation of the gradient-driving CSF secretion, CA2 and CA12 (*38*) (Fig. 5A). Staining revealed apical localization of AQP1, similar to that in vivo (Fig. 5B). Consistent with the specific role of ChP in the transport of folate and vitamin C, both vital for brain function (*39*, *40*), we also detected expression of specific transporters involved in the trafficking of these nutrients: SLC23A2 (vitamin C transporter) and SLC46A1 (folate transporter) (Fig. 5A).

To investigate whether the colorless fluid inside ChP organoids could represent an in vitro CSF-like fluid (iCSF), we performed mass spectrometry analysis of extracted fluid [five batches of H9, six batches of H1, and one batch of induced pluripotent stem cells (iPSCs) IMR-90] and compared the results with three different in vivo samples [human adult telencephalic

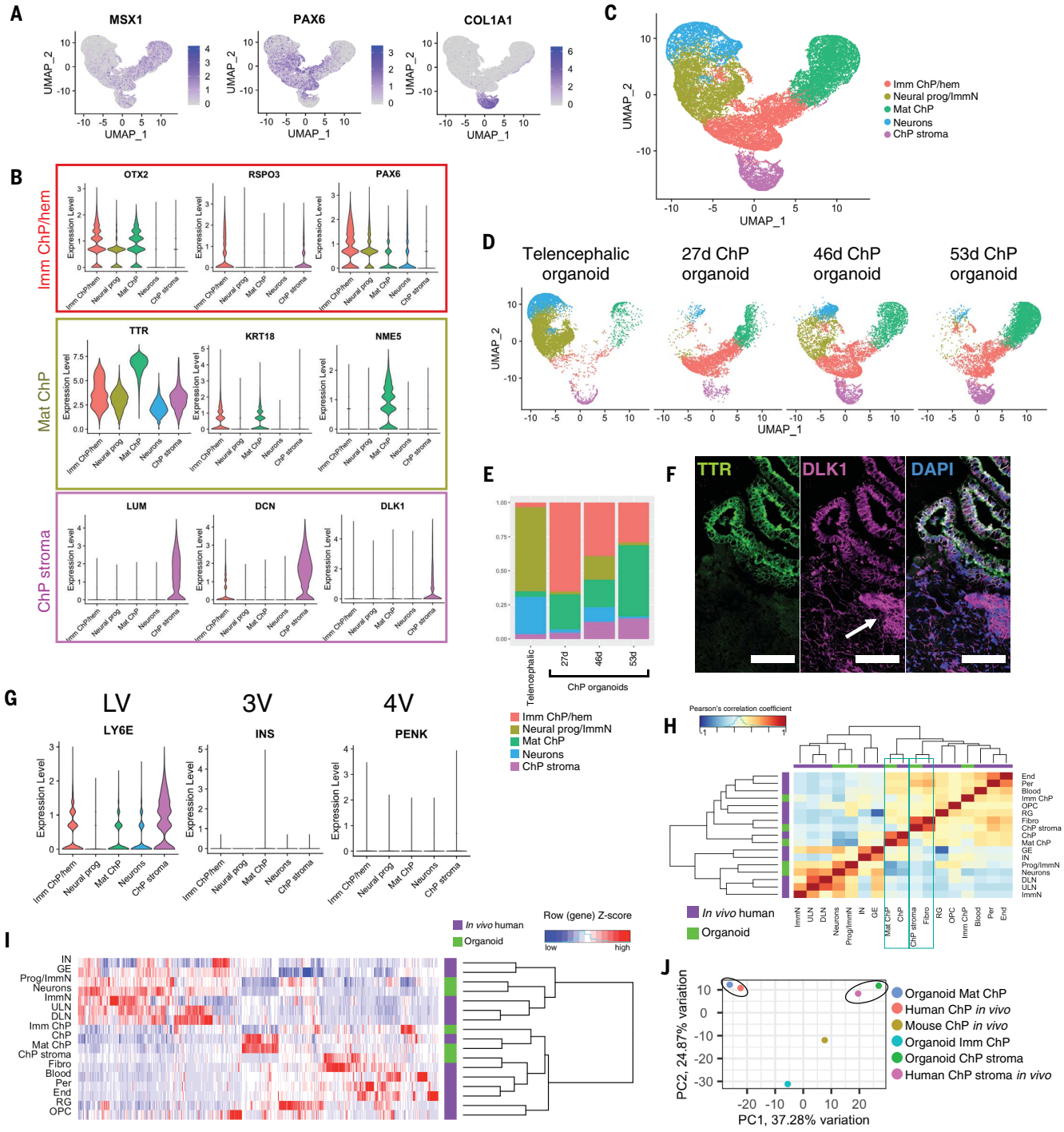

Fig. 2. ChP organoids closely recapitulate transcriptomic signature of human in vivo tissue. (**A**) Feature plots showing enrichment of genes involved in ChP development (MSX1, PAX6) and stromal marker COL1A1. (**B**) Violin plots of scRNA-seq analysis showing expression levels of ChP immature/hem (OTX2, RSPO3, PAX6), mature (TTR, KRT18, NME5), and stromal markers (LUM, DCN, DLK1). Imm ChP/hem, immature ChP/hem; Neural prog, neural progenitors; Mat ChP, mature ChP. (**C**) UMAP plot showing scRNA-seq clusters of combined samples. ImmN, immature neurons. (**D**) UMAP plots separated by samples showing progressive enrichment in ChP populations in ChP organoids compared to 55-day-old mixed telencephalic identity organoids. (**E**) Stacked bar chart showing relative proportion of clusters in each sample. (**F**) Confocal images of ChP organoids positive for TTR, DLK1, and DAPI in an adjacent stromal population (arrow). Scale bars, 100 μm. (**G**) Violin plots showing expression levels of regional ChP markers for lateral (LV, LY6E), third (3V, INS), and fourth (4V, PENK) ventricles. (**H**) Heatmap and dendrogram of Pearson's correlation coefficients across identified in vivo human dorsal telencephalon (*21*) and organoid clusters showing high similarity between in vivo and in vitro ChP clusters (green outline). ULN, upper-layer neurons; DLN, deep-layer neurons; IN, interneurons; GE, ganglionic eminences; Fibro, fibroblasts; RG, radial glia; OPC, oligodendrocyte progenitor cells; Per, pericytes; End, endothelial cells. (**I**) Heatmap and dendrogram of unbiased hierarchical clustering based on the 1000 most variable genes between organoid single-cell clusters and in vivo human brain single-cell clusters. (**J**) Principal components analysis (PCA) plot of scRNA-seq ChP clusters from mouse embryo, human fetal dorsal telencephalon, and ChP organoids, revealing higher similarity of ChP organoid clusters to human than to mouse ChP.

Corrected 9 July 2020. See full text.

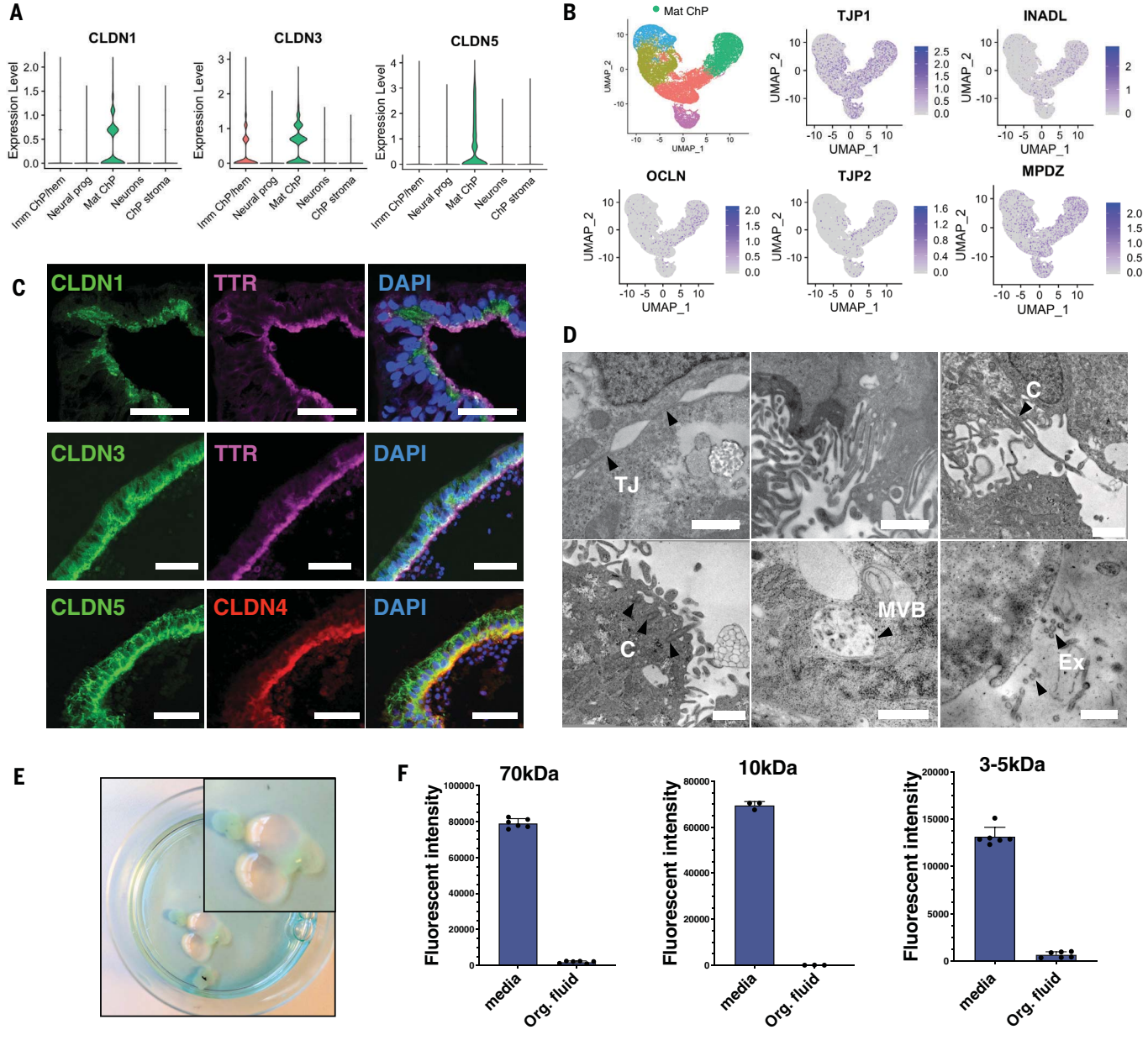

Fig. 3. ChP organoids form a tightly sealed barrier. (**A**) Violin plots showing expression levels of CLDN1, CLDN3, and CLDN5 in organoid cell clusters identified by scRNA-seq. (**B**) Feature plots showing enrichment in tight junction proteins TJP1 and TJP2, OCLN, INADL, and MPDZ in ChP immature and mature clusters. (**C**) Representative images of H1 ChP organoids (day 40) staining positive for TTR, CLDN1, CLDN3, CLDN4, CLDN5, and DAPI. Scale bars, 50 μm. (**D**) Electron micrographs showing tight junctions (TJ), microvilli (upper-middle panel), cilia (C), multivesicular bodies (MVB), and extracellular vesicles (Ex). Scale bars, 1 μm. The arrowheads point to the indicated component in each image. (**E**) Bright-field images of ChP organoids with clear, fluid-filled compartments despite incubation for 2 hours with 647-Alexafluor 10-kDa dextran (blue tint). (**F**) Fluorescent intensity in media and organoid fluid after 2-hour incubation with 70-kDa Oregon green–dextran, 10-kDa 647-Alexafluor dextran, and 3- to 5-kDa FITC-dextran. Error bars represent SEM.

CSF, mouse embryonic CSF at embryonic day 13.5 (E13.5), and fetal bovine CSF] (tables S3 and S4) and media. We detected 1618 proteins in ChP organoid iCSF, 851 of which were reliably detected in more than one iCSF sample (data S1). Gene ontology (GO) analysis revealed enrichment in cellular component (GO:CC) categories "extracellular vesicle" and "extracellular space" and biological process (GO:BP) categories "export from cell" and "secretion from cell" (Fig. 5C). The most abundant proteins in the iCSF largely overlapped with proteins present in vivo (fig. S9A). Indeed, of the 50 most abundant proteins detected in organoid iCSF, 49 were also detected in in vivo samples (Fig. 5D). Comparison of all the proteins detected revealed a large overlap between iCSF and in vivo samples (Fig. 5E and fig. S9B). We could detect clinically relevant biomarkers, for example, APOE, insulin-like growth factor binding protein 7 (IGFBP7), serpin family F member 1 (SERPINF1), and parkinsonism associated deglycase (PARK7) (table S5).

To ascertain the similarity of organoid iCSF to CSF in vivo, we examined proteins detected reproducibly in in vivo samples but not in organoid iCSF (fig. S9C), because these could be factors that the organoid failed to produce. Proteins detected exclusively in the in vivo CSF samples showed enrichment in GO:CC "blood

Corrected 9 July 2020. See full text.

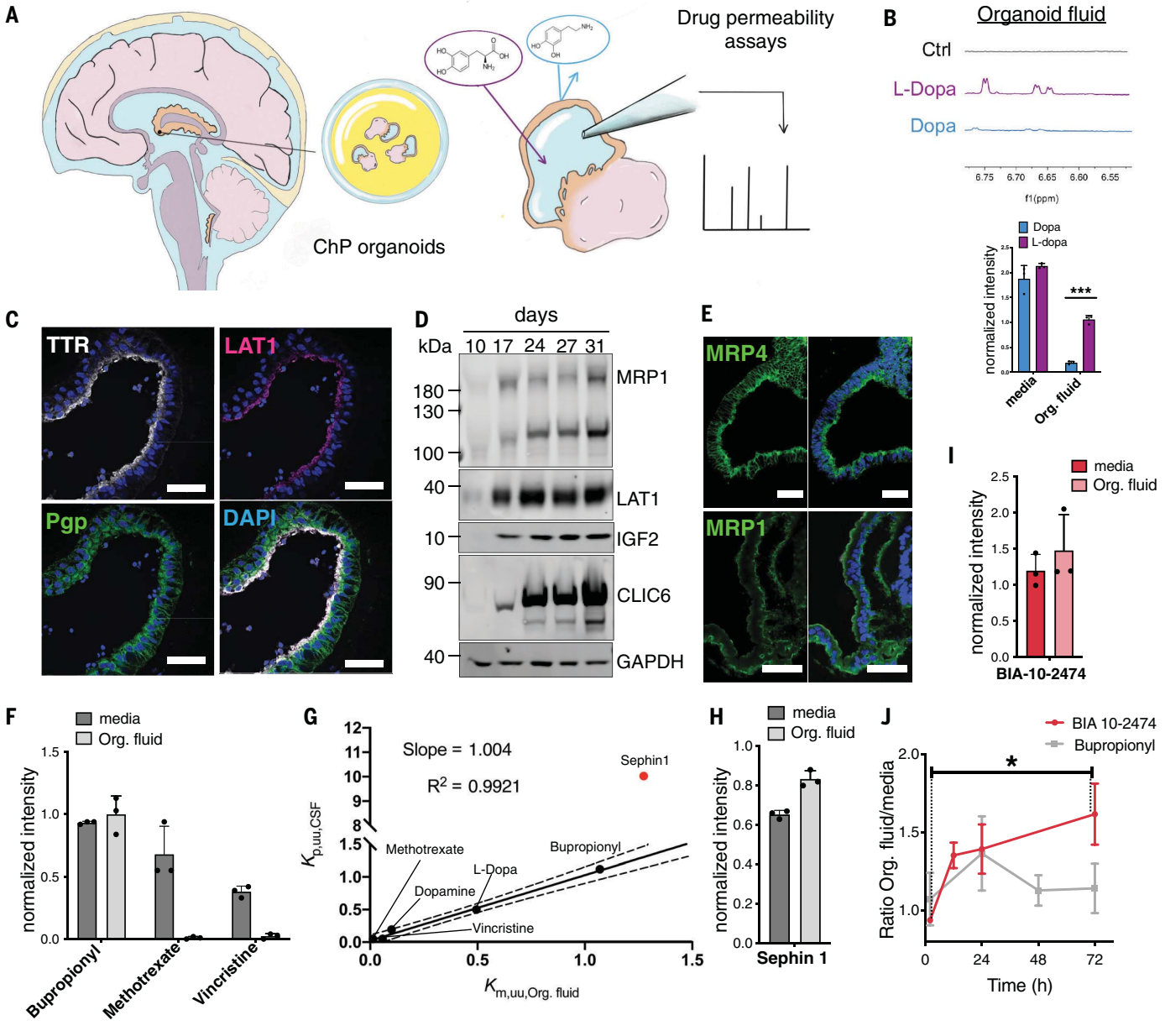

Fig. 4. ChP organoids predict CNS permeability of small molecules. (**A**) Schematic of CNS drug permeability measurement in ChP organoids. (**B**) Top: NMR spectra of organoid fluid on application of dopa, L-dopa, or no drug (Ctrl) measured after 2-hour incubation. ppm, parts per million. Bottom: Quantifications of above NMR spectra in media and organoid fluid. ***$P < 0.001$. Error bars represent SEM. (**C**) Representative images of ChP organoids stained for TTR, LAT1, Pgp, and DAPI. Scale bars, 50 μm. (**D**) Immunoblot for ChP transporters MRP1, LAT1, CLIC6, and secreted protein IGF2, and the loading control GAPDH of ChP organoid lysates (day 10 to day 31). (**E**) Confocal images of ChP organoids stained for transporters MRP4 and MRP1. Scale bars, 50 μm. (**F**) Relative quantifications of NMR spectra of bupropionyl, methotrexate, and vincristine in media and organoid fluid after 2 hours. Error bars represent SEM. (**G**) Scatter plot with linear regression showing correlation ($R^2 = 0.9921$; slope = 1.004) between in vivo CSF/plasma ratio ($K_{p,uu,CSF}$) and in vitro organoid fluid/media ratio ($K_{m,uu,Org.fluid}$) of unbound drugs (table S2). In contrast to other drugs shown, Sephin 1 (red dot) in vivo CSF/plasma measurement is the reported value from mice (*32*). (**H**) Relative quantifications of NMR spectra of Sephin 1 in media and organoid fluid after 2 hours. Error bars represent SEM. (**I**) Relative quantifications of NMR spectra of BIA 10-2474 in media and organoid fluid after 2 hours. (**J**) Time course analysis of the ratio of BIA 10-2474 and bupropionyl in organoid fluid to media at 2, 12, 24, and 72 hours. Error bars represent SEM. *$P < 0.05$. (All drugs were tested in $n = 3$ independent experiments; see table S1.)

microparticle," GO:BP "platelet degranulation," and GO category molecular function (GO:MF) "oxygen carrier activity" (fig. S9D). This suggests that these are factors coming from the blood, either through transport across the B-CSF-B or as collection artifacts through blood contamination. These would not be expected to be present in ChP organoids because they lack a vascular system and blood and hence represent the ChP in isolation.

ChP-CSF organoids progressively mature over time

ChP organoids progressively expressed more mature markers (Fig. 2, D and E). To test whether the composition of iCSF also matured

Corrected 9 July 2020. See full text.

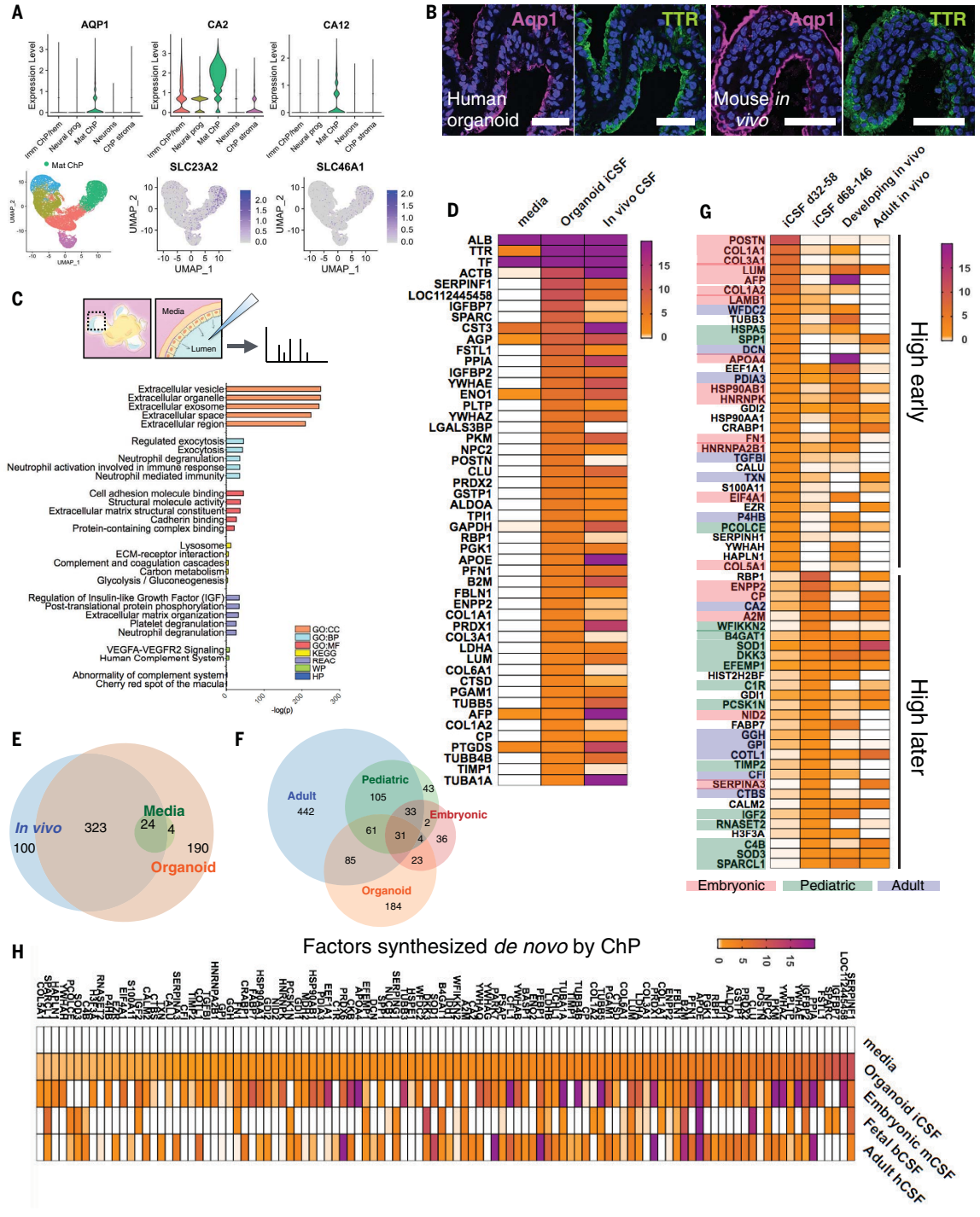

Fig. 5. ChP organoids secrete human CSF proteins and progressively mature to a postnatal state. (**A**) Top: Violin plots showing expression levels of water transporter AQP1 and CSF secretion enzymes CA2 and CA12 in scRNA-seq clusters. Bottom: Feature plots showing enrichment in SLC23A2 (vitamin C transporter) and SLC46A1 (folate transporter) in scRNA-seq clusters. (**B**) Confocal images of H1 ChP organoid at day 40 and in vivo ChP from a mouse embryo (E18.5) stained for Aqp1 and TTR. Scale bars, 50 μm. (**C**) gProfileR (*46*) analysis of proteins detected in iCSF from at least two ChP organoid samples, showing significant ($P < 0.05$) enrichments for GO categories cellular component (GO:CC), molecular function (GO:MF), and biological process (GO:BP), Kyoto Encyclopedia of Genes and Genomes (KEGG), REAC, WikiPathways (WP), and Human Phenotype (HP) databases. (**D**) Color-coded heatmap showing relative abundance (emPAI values) of proteins detected in organoid iCSF from at least two organoid batches (five batches of H9, six batches of H1, and one iPSC batch; table S3) and with a mean emPAI ≥ 1 in organoids. Corresponding values are shown for the media, the mean of the 12 organoid samples, and the mean of three in vivo CSF samples: human adult CSF, bovine fetal CSF, and embryonic mouse CSF (E12.5 to 13.5) (table S4). (**E**) Venn diagram of all proteins detected with an emPAI ≥ 1 in any sample. Proteins were assigned to each group in which they were detectable at any level. (**F**) Venn diagram of proteins detected in at least two iCSF samples and with an emPAI ≥ 1 in at least one. Overlap is shown for proteins detected in datasets of human adult CSF (*47*), pediatric CSF from healthy controls (*48*), and human embryonic CSF (*49*). (**G**) Color-coded heatmap of protein emPAI levels showing abundant iCSF proteins (emPAI ≥ 1 in early day 32 to day 58 or late day 68 to day 146 stage organoids) shared with in vivo samples (split into developing and adult). Proteins are highlighted and color coded according to the earliest stage human in vivo CSF dataset in which they are detected from the following published datasets: human adult CSF (*47*), pediatric CSF (*48*), and embryonic CSF (*49*). (**H**) emPAI heatmap of proteins reproducibly (more than one iCSF sample) and abundantly (emPAI ≥ 1 in early day 32 to day 58 or late day 68 to day 146 stage organoids) detected in iCSF but not in media and shared with at least one in vivo sample, which are considered de novo ChP-derived CSF proteins. mCSF, mouse CSF; bCSF, bovine CSF; hCSF, human CSF.

over time, we compared proteins in iCSF with published datasets of normal human embryonic, pediatric, and adult CSF (data S2). We observed overlap with all three human age ranges, including a number of genes shared with the more mature time points (Fig. 5F). A number of proteins in iCSF changed abundance over time, with a marked shift between the day 58 and 68 time points (fig. S9A). We further analyzed early (abundant before day 60) and late (abundant after day 60) proteins (fig. S10A). Whereas early abundant proteins overlapped with embryonic and fetal in vivo samples and datasets, late abundant proteins overlapped more with pediatric and adult stages (Fig. 5G).

We next examined factors known to exhibit changes in CSF levels over time (fig. S10B). Abundant extracellular matrix proteins (laminin, fibronectin, and collagens) were shared with human embryonic CSF at the earliest time points (Fig. 5G and fig. S10B). Insulin-like growth factor 2 (IGF2) is an important signaling factor in developing CSF (*2*). We observed a number of IGF factors present in iCSF, enriched in the Reactome (REAC) category "regulation of insulin-like growth factor" (Fig. 5C). IGF2 was highly abundant, with levels dropping off at the latest stage tested of 146 days (fig. S10, B and C), which closely matched the pattern in vivo, where IGF2 was detected in developing embryonic, fetal, and pediatric CSF (Fig. 5G).

We next examined proteins whose expression should increase in postnatal and adult CSF. We observed a number of lipoproteins in organoid iCSF—such as APOE, clusterin (CLU), APOD, and phospholipid transfer protein (PLTP)—which increased over time and were shared with adult in vivo CSF (fig. S10B). Similarly, we observed a marked presence of lipid droplets at later stages (fig. S10D). Finally, we observed a number of other markers increasing with time, including retinol binding protein 1 (RBP1), ceruloplasmin (CP), and complement proteins (C1R and C4B) (fig. S10B). Together, these results suggest that late-stage organoids (older than 60 days) recapitulate functionality of pediatric and even adult ChP, with production of more mature CSF-like fluid by 100 days.

Identification of the tissue source of key CSF components

Organoids represent tissues in isolation, lacking cell types such as vasculature and an immune system. Although this can be a limitation, we viewed this as a strength when examining secretion of a biological fluid such as CSF. This isolation can be leveraged to reveal factors from external sources, such as surrounding brain tissue or filtered from the blood, versus those made de novo by the ChP itself. To explore which CSF factors may be filtered, rather than made de novo, we examined iCSF proteins also present in fresh media (fig. S10E). Many of these factors were shared with in vivo CSF samples, suggesting that these may also be filtered into the CSF in vivo.

CSF composition may also be influenced by surrounding brain tissue. We therefore examined organoid fluid from telencephalic organoids of mixed identity, which would include the ChP. The fluid largely overlapped that of pure ChP organoids (fig. S10F), suggesting that CSF composition is primarily determined by ChP secretion. However, a number of proteins were specific to mixed-identity organoids, 11 of which were shared with in vivo samples (fig. S10G). These may represent bona fide brain-derived factors such as secretogranin-1 (CHGB), a neuroendocrine secretory protein, and NDRG2, an astrocyte-expressed protein implicated in neurite outgrowth. The vast majority of proteins (1589 of 1618) were not shared with media, suggesting de novo ChP secretion (Fig. 5H). Overall, these findings suggest that CSF composition is largely dictated by ChP secretion, with a subset of components being filtered from the blood and produced by surrounding brain tissue.

Merging proteomic and transcriptomic data reveals cell type–specific secretion and identifies previously unidentified ChP epithelial subtypes

To identify specific ChP cell types responsible for secretion of CSF components, we used scRNA-seq to examine expression of key factors present in iCSF. The developmental signaling factor IGF2 was expressed in the ChP stroma (fig. S11A) but also later within the mature ChP epithelium (fig. S11, B and C). More mature factors were specifically expressed within the mature ChP epithelium (fig. S11, A and D), whereas biomarkers exhibited varying expression patterns across ChP clusters (fig. S11E). These findings provide insight into which cells within the ChP produce key secreted proteins.

Although several secreted proteins were expressed broadly among mature ChP cells (i.e., PLTP, CP), others such as IGF2, COL1A2, and C1R exhibited more restricted expression (fig. S11A), suggesting the existence of ChP epithelial subtypes involved in the secretion of specific CSF components. We therefore performed subclustering of the mature ChP cluster and identified four prominent clusters (Fig. 6A). Differential gene expression analysis of these clusters revealed a cluster expressing not only markers of ChP epithelium (AQP1 and CLDN5) but also high levels of mitochondrial genes (Fig. 6, B and C, and fig. S12, A and B). The second most abundant cluster instead showed marked down-regulation of mitochondrial genes but up-regulation of microtubule cytoskeletal and ciliary assembly factors (Fig. 6, B and C).

Some studies of ChP ultrastructure reported the existence of "dark" and "light" cells (*7*), but nothing is known about their molecular identities. Dark cells, or "mitochondria-rich cells," have also been observed in other secretory organs (*41*). These cells also lack cilia. We therefore hypothesized that the two most abundant clusters of the ChP epithelium may be dark and light epithelial cells with opposite expression of mitochondrial and ciliary genes. Electron micrographs revealed abundant dark cells with interspersed light cells with a ciliary basal body (Fig. 6D). We observed nonhomogeneous expression of the mitochondrial marker CARD19, the ciliary transcription factor FOXJ1, and the ciliary markers ARL13B and CCDC67 in subsets of cells (Fig. 6, E and F, and fig. S12C). These results provide a first look at the molecular and cellular hallmarks of dark and light ChP epithelial cells.

Closer examination of differential gene expression in the third cluster of ChP epithelial cells revealed markers typical of myoepithelial cells (Fig. 6, B and C, and fig. S12, A and B), a cell type described in secretory glands. These cells express contractile actin and myosin, similar to smooth muscle cells (α-SMA), yet are bona fide epithelial cells expressing markers such as keratin 17 (KRT17) (Fig. 6, B and C). Furthermore, staining for α-SMA and transgelin (TAGLN) revealed their expression in a subset of cells within the epithelium (Fig. 6G). Finally, we observed a cluster of cells expressing markers of DNA replication and the cell cycle (Fig. 6, B and C, and fig. S12, A and B), possibly indicating dividing cells. Indeed, we could observe occasional dividing PH3-positive cells in mature ChP epithelium, decreasing over time (fig. S12D). These findings suggest the presence of a limited number of dividing mature epithelial cells, as well as contractile cells, that had not been described in the ChP and may help promote CSF secretion, similar to secretory glands elsewhere in the body.

We next took an unbiased approach to explore cell type–specific secretion by looking at overlapping genes between mass spectrometry analysis and scRNA-seq (Fig. 7A and data S3). We also examined specific genes of interest in this context, such as IGF2, which was restricted to dark cells of the ChP epithelium (Fig. 7B and fig. S13A), consistent with its staining pattern (Fig. 7C). The expression of the more mature marker RBP1 in dark cells (Fig. 7A) was also further confirmed by immunostaining (fig. S13B). Finally, a number of biomarkers were specifically produced by epithelial subtypes, including SERPINF1, IGFBP2, PARK7, and APOE (Fig. 7A and fig. S13C). Overall, these findings provide insight into specific cell types and their secretions within the ChP epithelium.

Identification of CSF proteins secreted by the developing human ChP

ChP organoids provide a model system for developing human ChP and CSF. We therefore

Corrected 9 July 2020. See full text.

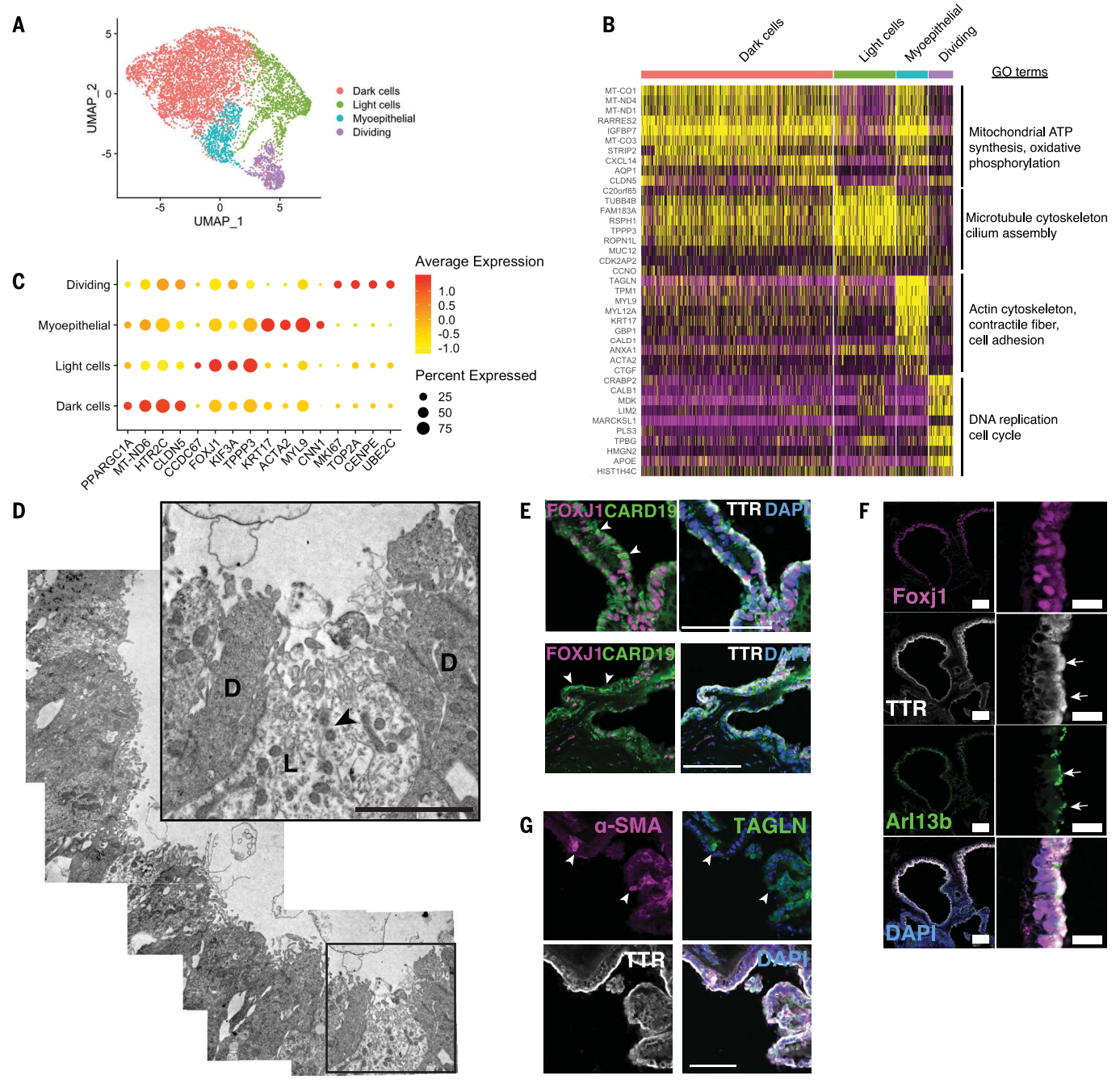

Fig. 6. Identification and molecular characterization of ChP epithelial subtypes. (**A**) UMAP plot showing subclustering of the mature ChP epithelial cluster identified by scRNA-seq. (**B**) Heatmap of top 10 differentially up-regulated transcripts in the four subclusters identified and the major GO terms enriched for each cluster. (**C**) Dot plot showing average expression and percentage of cells expressing the displayed enriched genes identified by scRNA-seq. (**D**) Electron micrographs showing dark (D) and light (L) cells on the ChP epithelium in organoids. The arrowhead points to a basal body in a light cell. Scale bar, 40 μm. (**E**) Representative confocal images of H1 ChP organoid (day 82) stained for mitochondrial marker CARD19, ciliated cell marker FOXJ1, TTR, and DAPI. Scale bars, 100 μm. (**F**) Confocal images of H1 ChP organoid (day 46) stained for Foxj1, Arl13b (cilia), TTR, and DAPI. Scale bars, 100 μm (magnified-view scale bars, 20 μm). The arrows point at tufts of cilia on the ChP apical side. (**G**) Representative confocal images of H1 ChP organoid (day 82) stained for alpha-smooth muscle actin (α-SMA), transgelin (TAGLN), TTR, and DAPI. Scale bar, 100 μm.

focused on iCSF-specific factors. Because none of the in vivo samples tested here were from developing human CSF, any CSF components specific to the ChP organoids could represent either in vitro–specific or human-specific developmental factors. We identified 24 proteins that were reproducibly abundant in ChP iCSF but absent in mouse and bovine developing CSF as well as adult human CSF (Fig. 7D). We then queried published datasets of human developing CSF from fetal and pediatric stages, which revealed some overlap with known human developmental CSF factors, whereas others had not been observed before but are predicted to be secreted proteins (Fig. 7, D and E).

One human-specific developmental secreted protein, LGALS3BP, stood out because it has also been identified in outer radial glial progenitors

Corrected 9 July 2020. See full text.

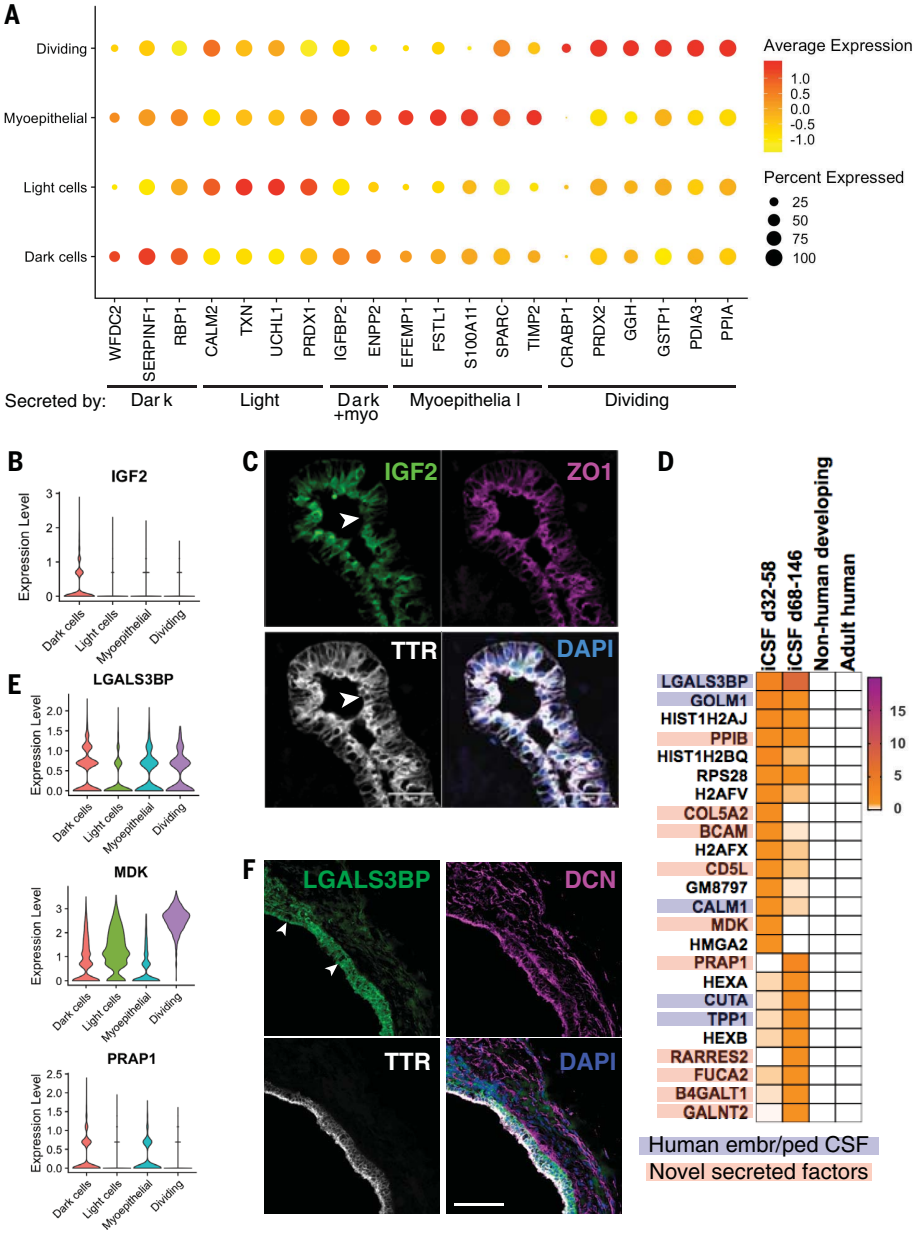

Fig. 7. Identification of previously unidentified factors secreted by distinct ChP epithelial subtypes. (**A**) Dot plot showing average expression and percentage of cells expressing factors overlapping between iCSF-detected proteins and differentially expressed genes within the four subclusters (data S3). myo, myoepithelial. (**B**) Violin plot showing expression of IGF2 in ChP epithelial subtypes identified by scRNA-seq. (**C**) Representative confocal images of H9 ChP organoid (day 50) stained for IGF2, ZO1, TTR, and DAPI. Scale bars, 50 μm. The arrowheads point to IGF2-negative cells. (**D**) Color-coded heatmap showing proteins reproducibly (detected in more than one iCSF sample) and abundantly (emPAI ≥ 1 in early day 32 to day 58 or late day 68 to day 146 stage organoids) detected in iCSF but not in media or in in vivo developing mouse or bovine CSF or in adult human CSF. Highlighted and color coded accordingly are proteins detected in published datasets of human embryonic (embr) (*49*) or pediatric (ped) CSF (*48*) and unknown factors predicted to be secreted (GeneCards database). (**E**) Violin plots showing expression levels of secreted proteins identified exclusively in organoid iCSF: LGALS3BP, MDK, and PRAP1. (**F**) Representative confocal images of H1 ChP organoid (day 56) stained for LGALS3BP, DCN, TTR, and DAPI. The arrowheads point to LGALS3BP punctae. Scale bar, 100 μm.

of the human fetal brain (*42*). We therefore examined the expression of this factor further and found it to be present in neural progenitors (fig. S13D) but more abundant in the ChP (fig. S13E), specifically in dark, myoepithelial, and dividing cells, but less in light cells (Fig. 7E). Immunohistochemistry also revealed abundant, broad staining throughout the ChP epithelium (Fig. 7F). These findings highlight a number of promising candidate signaling proteins that may play important roles in human brain development.

Discussion

We present ChP organoids for the investigation of development and function of the human ChP. Using this in vitro organoid model, we are able to demonstrate the two key functions of the ChP: barrier formation and CSF secretion. ChP organoids are selective to highly similar small molecules. This model matches the selectivity of the human blood-CNS barrier in vivo, and it can predict CNS permeability of both known and new drug compounds.

There is an increasing demand for more effective CNS drugs. New drugs too often progress to clinical trial before failing for lack of efficacy, inability to cross into the CNS, or limited translatability from animal models (*43*). ChP organoids could be exploited for preclinical testing to identify new modes of drug entry into the CNS.

We further show that the fluid secreted by ChP organoids represents an authentic biological fluid, separate from the media, that exhibits a high degree of similarity to CSF in vivo. The organoids and CSF-like fluid also mature over time, reaching a state highly similar to postnatal stages and even adulthood. This would enable the study of disease-related biomarkers, whose functions are still not well understood. The ChP is relatively understudied, but it is garnering increasing attention because of its important roles in development and diseases such as neurodegeneration.

Finally, we have leveraged the isolated nature of ChP organoids to identify and molecularly describe previously unidentified ChP epithelial cell types and to identify their specific CSF secretions. With this model, we were able to disentangle CSF components that are specifically made by the ChP from those transported across or generated by the surrounding brain tissue. This revealed a number of developmental

factors and human-specific signaling proteins that may play key roles in brain development and homeostasis. We are hopeful that with this information in hand, further studies can begin to illuminate the vital functions of the ChP in brain development and disease.

Materials and methods summary

Cerebral and ChP organoid culture conditions

Stem Cell Technologies Cerebral Organoid kit (catalog nos. 08570 and 08571) reagents were used for the generation of cerebral and ChP organoids. For ChP patterning, 3 μM CHIR and 20 ng/ml BMP4 were added in maturation media on day 10 until day 17. Detailed methods for the organoid differentiation protocol are included in the supplementary materials.

Immunostaining and immunoblotting

Organoids were fixed in 4% paraformaldehyde (PFA) overnight at 4°C and then moved to 30% sucrose buffer. Organoids were then embedded in gelatin and sectioned as previously described (*44*). After blocking and permeabilization, sections were incubated overnight with primary antibody. A detailed list of antibodies used is included in the supplementary materials. Images were acquired using a Zeiss LSM 780 confocal microscope (Carl Zeiss) and prepared using Fiji (NIH). Detailed methods for sample preparation and imaging by electron microscopy are included in the supplementary materials. For immunoblotting, organoids were homogenized in radioimmunoprecipitation assay (RIPA) buffer. Protein samples were loaded into a SDS–polyacrylamide gel electrophoresis (SDS-PAGE) gel. Membranes were imaged using a Li-COR Odyssey CLx Infrared Imaging System. Detailed methods for preparation of cytosol-enriched fractions are included in the supplementary materials.

scRNA-seq

Single-cell dissociation was performed by pooling two organoids for each condition: 55-day H9 telencephalic organoids, 27-day H1 ChP, 46-day H1 ChP, and 53-day H1 ChP. Dissociated cells were resuspended in 0.04% bovine serum albumin (BSA) in phosphate-buffered saline (PBS) to load 16,000 cells for each sample on the 10X Chromium system (10X Genomics). Detailed methods for scRNA-seq, bioinformatic analysis, and comparison with in vivo datasets are included in the supplementary materials.

Samples for mass spectrometry and NMR analysis

iCSF was collected using a pulled glass microcapillary attached to filter and tubing using controlled suction. In vivo samples were human adult telencephalic CSF (Caltag-Medsystem), bovine fetal CSF (bCSF, BioIVT), and embryonic mouse CSF from E12.5 to E13.5 telencephalic ventricles. Detailed methods for mass spectrometry analysis, NMR analysis, and comparison between in vivo and in vitro drug permeability are included in the supplementary materials.

REFERENCES AND NOTES

1. M. P. Lun, E. S. Monuki, M. K. Lehtinen, Development and functions of the choroid plexus-cerebrospinal fluid system. *Nat. Rev. Neurosci.* **16**, 445–457 (2015). doi: 10.1038/nrn3921; pmid: 26174708
2. M. K. Lehtinen, C. A. Walsh, Neurogenesis at the brain-cerebrospinal fluid interface. *Annu. Rev. Cell Dev. Biol.* **27**, 653–679 (2011). doi: 10.1146/annurev-cellbio-092910-154026; pmid: 21801012
3. V. Silva-Vargas, A. R. Maldonado-Soto, D. Mizrak, P. Codega, F. Doetsch, Age-dependent niche signals from the choroid plexus regulate adult neural stem cells. *Cell Stem Cell* **19**, 643–652 (2016). doi: 10.1016/j.stem.2016.06.013; pmid: 27452173
4. M. P. Lun *et al.*, Spatially heterogeneous choroid plexus transcriptomes encode positional identity and contribute to regional CSF production. *J. Neurosci.* **35**, 4903–4916 (2015). doi: 10.1523/JNEUROSCI.3081-14.2015; pmid: 25810521
5. J. F. Ghersi-Egea *et al.*, Molecular anatomy and functions of the choroidal blood-cerebrospinal fluid barrier in health and disease. *Acta Neuropathol.* **135**, 337–361 (2018). doi: 10.1007/s00401-018-1807-1; pmid: 29368213
6. Z. Redzic, Molecular biology of the blood-brain and the blood-cerebrospinal fluid barriers: Similarities and differences. *Fluids Barriers CNS* **8**, 3 (2011). doi: 10.1186/2045-8118-8-3; pmid: 21349151
7. G. J. Dohrmann, P. C. Bucy, Human choroid plexus: A light and electron microscopic study. *J. Neurosurg.* **33**, 506–516 (1970). doi: 10.3171/jns.1970.33.5.0506; pmid: 4920907
8. M. A. Lancaster *et al.*, Cerebral organoids model human brain development and microcephaly. *Nature* **501**, 373–379 (2013). doi: 10.1038/nature12517; pmid: 23995685
9. G. Quadrato *et al.*, Cell diversity and network dynamics in photosensitive human brain organoids. *Nature* **545**, 48–53 (2017). doi: 10.1038/nature22047; pmid: 28445462
10. S. P. Paşca, The rise of three-dimensional human brain cultures. *Nature* **553**, 437–445 (2018). doi: 10.1038/nature25032; pmid: 29364288
11. H. Sakaguchi *et al.*, Generation of functional hippocampal neurons from self-organizing human embryonic stem cell-derived dorsomedial telencephalic tissue. *Nat. Commun.* **6**, 8896 (2015). doi: 10.1038/ncomms9896; pmid: 26573335
12. R. M. Fame, M. K. Lehtinen, Emergence and developmental roles of the cerebrospinal fluid system. *Dev. Cell* **52**, 261–275 (2020). doi: 10.1016/j.devcel.2020.01.027; pmid: 32049038
13. M. A. Lancaster *et al.*, Guided self-organization and cortical plate formation in human brain organoids. *Nat. Biotechnol.* **35**, 659–666 (2017). doi: 10.1038/nbt.3906; pmid: 28562594
14. S. L. Giandomenico *et al.*, Cerebral organoids at the air-liquid interface generate diverse nerve tracts with functional output. *Nat. Neurosci.* **22**, 669–679 (2019). doi: 10.1038/s41593-019-0350-2; pmid: 30886407
15. M. Watanabe *et al.*, BMP4 sufficiency to induce choroid plexus epithelial fate from embryonic stem cell-derived neuroepithelial progenitors. *J. Neurosci.* **32**, 15934–15945 (2012). doi: 10.1523/JNEUROSCI.3227-12.2012; pmid: 23136431
16. D. S. Currle, X. Cheng, C. M. Hsu, E. S. Monuki, Direct and indirect roles of CNS dorsal midline cells in choroid plexus epithelia formation. *Development* **132**, 3549–3559 (2005). doi: 10.1242/dev.01915; pmid: 15975937
17. M. K. Lehtinen *et al.*, The choroid plexus and cerebrospinal fluid: Emerging roles in development, disease, and therapy. *J. Neurosci.* **33**, 17553–17559 (2013). doi: 10.1523/JNEUROSCI.3258-13.2013; pmid: 24198345
18. S. A. Liddelow, Development of the choroid plexus and blood-CSF barrier. *Front. Neurosci.* **9**, 32 (2015). doi: 10.3389/fnins.2015.00032; pmid: 25784848
19. M. Sathyanesan *et al.*, A molecular characterization of the choroid plexus and stress-induced gene regulation. *Transl. Psychiatry* **2**, e139–e9 (2012). doi: 10.1038/tp.2012.64; pmid: 22781172
20. N. Dani *et al.*, A cellular and spatial map of the choroid plexus across brain ventricles and ages. bioRxiv 627539 [Preprint]. 5 May 2019; https://doi.org/10.1101/627539.
21. T. J. Nowakowski *et al.*, Spatiotemporal gene expression trajectories reveal developmental hierarchies of the human cortex. *Science* **358**, 1318–1323 (2017). doi: 10.1126/science.aap8809; pmid: 29217575
22. J. Cao *et al.*, The single-cell transcriptional landscape of mammalian organogenesis. *Nature* **566**, 496–502 (2019). doi: 10.1038/s41586-019-0969-x; pmid: 30787437
23. R. Duelli, B. E. Enerson, D. Z. Gerhart, L. R. Drewes, Expression of large amino acid transporter LAT1 in rat brain endothelium. *J. Cereb. Blood Flow Metab.* **20**, 1557–1562 (2000). doi: 10.1097/00004647-200011000-00005; pmid: 11083230
24. H. Uchino *et al.*, Transport of amino acid-related compounds mediated by L-type amino acid transporter 1 (LAT1): Insights into the mechanisms of substrate recognition. *Mol. Pharmacol.* **61**, 729–737 (2002). doi: 10.1124/mol.61.4.729; pmid: 11901210
25. R. Durso *et al.*, Variable absorption of carbidopa affects both peripheral and central levodopa metabolism. *J. Clin. Pharmacol.* **40**, 854–860 (2000). doi: 10.1177/00912700022009585; pmid: 10934669
26. V. V. Rao *et al.*, Choroid plexus epithelial expression of MDR1 P glycoprotein and multidrug resistance-associated protein contribute to the blood–cerebrospinal-fluid drug-permeability barrier. *Proc. Natl. Acad. Sci. U.S.A.* **96**, 3900–3905 (1999). doi: 10.1073/pnas.96.7.3900; pmid: 10097135
27. C. J. Ek *et al.*, Efflux mechanisms at the developing brain barriers: ABC-transporters in the fetal and postnatal rat. *Toxicol. Lett.* **197**, 51–59 (2010). doi: 10.1016/j.toxlet.2010.04.025; pmid: 20466047
28. Y. Uchida, Z. Zhang, M. Tachikawa, T. Terasaki, Quantitative targeted absolute proteomics of rat blood-cerebrospinal fluid barrier transporters: Comparison with a human specimen. *J. Neurochem.* **134**, 1104–1115 (2015). doi: 10.1111/jnc.13147; pmid: 25951748
29. S. G. Summerfield, Y. Zhang, H. Liu, Examining the uptake of central nervous system drugs and candidates across the blood-brain barrier. *J. Pharmacol. Exp. Ther.* **358**, 294–305 (2016). doi: 10.1124/jpet.116.232447; pmid: 27194478
30. L. Angelov *et al.*, Blood-brain barrier disruption and intra-arterial methotrexate-based therapy for newly diagnosed primary CNS lymphoma: A multi-institutional experience. *J. Clin. Oncol.* **27**, 3503–3509 (2009). doi: 10.1200/JCO.2008.19.3789; pmid: 19451444
31. E. Zylber-Katz *et al.*, Pharmacokinetics of methotrexate in cerebrospinal fluid and serum after osmotic blood-brain barrier disruption in patients with brain lymphoma. *Clin. Pharmacol. Ther.* **67**, 631–641 (2000). doi: 10.1067/mcp.2000.106932; pmid: 10872645
32. I. Das *et al.*, Preventing proteostasis diseases by selective inhibition of a phosphatase regulatory subunit. **348**, 239–243 (2015).
33. C. H. I. H. Wong, K. W. E. I. Siah, A. W. Lo, Estimation of clinical trial success rates and related parameters. *Biostatistics* **20**, 273–286 (2019). doi: 10.1093/biostatistics/kxx069; pmid: 29394327
34. R. Kaur, P. Sidhu, S. Singh, What failed BIA 10-2474 phase I clinical trial? Global speculations and recommendations for future phase I trials. *J. Pharmacol. Pharmacother.* **7**, 120–126 (2016). doi: 10.4103/0976-500X.189661; pmid: 27651707
35. K. Otrubova, C. Ezzili, D. L. Boger, The discovery and development of inhibitors of fatty acid amide hydrolase (FAAH). *Bioorg. Med. Chem. Lett.* **21**, 4674–4685 (2011). doi: 10.1016/j.bmcl.2011.06.096; pmid: 21764305
36. D. Butler, E. Callaway, Scientists in the dark after French clinical trial proves fatal. *Nature* **529**, 263–264 (2016). doi: 10.1038/nature.2016.19189; pmid: 26791697
37. S. M. Bird, R. A. Bailey, A. P. Grieve, S. Senn, Statistical issues in first-in-human studies on BIA 10-2474: Neglected comparison of protocol against practice. *Pharm. Stat.* **16**, 100–106 (2017). doi: 10.1002/pst.1801; pmid: 28206702
38. E. Kida *et al.*, Carbonic anhydrase II in the developing and adult human brain. *J. Neuropathol. Exp. Neurol.* **65**, 664–674 (2006). doi: 10.1097/01.jnen.0000225905.52002.3e; pmid: 16825953
39. J. B. Wollack *et al.*, Characterization of folate uptake by choroid plexus epithelial cells in a rat primary culture model. *J. Neurochem.* **104**, 1494–1503 (2008). doi: 10.1111/j.1471-4159.2007.05095.x; pmid: 18086128
40. V. Ulloa *et al.*, Basal sodium-dependent vitamin C transporter 2 polarization in choroid plexus explant cells in normal or scorbutic conditions. *Sci. Rep.* **9**, 14422 (2019). doi: 10.1038/s41598-019-50772-2; pmid: 31594969
41. A. Roy, M. M. Al-bataineh, N. M. Pastor-Soler, Collecting duct intercalated cell function and regulation. *Clin. J. Am. Soc. Nephrol.* **10**, 305–324 (2015). pmid: 25632105

42. A. A. Pollen *et al*., Molecular identity of human outer radial glia during cortical development. *Cell* **163**, 55–67 (2015). doi: 10.1016/j.cell.2015.09.004; pmid: 26406371
43. J.-M. Nicolas, in *Blood-Brain Barrier in Drug Discovery: Optimizing Brain Exposure of CNS Drugs and Minimizing Brain Side Effects for Peripheral Drugs*, L. Di, E. H. Kerns, Eds. (Wiley, 2015).
44. M. A. Lancaster, J. A. Knoblich, Generation of cerebral organoids from human pluripotent stem cells. *Nat. Protoc.* **9**, 2329–2340 (2014). doi: 10.1038/nprot.2014.158; pmid: 25188634
45. J. A. Miller *et al*., Transcriptional landscape of the prenatal human brain. *Nature* **508**, 199–206 (2014). doi: 10.1038/nature13185; pmid: 24695229
46. U. Raudvere *et al*., g:Profiler: a web server for functional enrichment analysis and conversions of gene lists (2019 update). *Nucleic Acids Res.* **47**, W191–W198 (2019). doi: 10.1093/nar/gkz369; pmid: 31066453
47. L. Dayon *et al*., Proteomes of paired human cerebrospinal fluid and plasma: Relation to blood-brain barrier permeability in older adults. *J. Proteome. Res.* **18**, 1162–1174 (2019). doi: 10.1021/acs.jproteome.8b00809; pmid: 30702894
48. L. Guo, H. Ren, H. Zeng, Y. Gong, X. Ma, Proteomic analysis of cerebrospinal fluid in pediatric acute lymphoblastic leukemia patients: A pilot study. *OncoTargets Ther.* **12**, 3859–3868 (2019). doi: 10.2147/OTT.S193616; pmid: 31190885
49. M. D. Zappaterra *et al*., A comparative proteomic analysis of human and rat embryonic cerebrospinal fluid. *J. Proteome Res.* **6**, 3537–3548 (2007). doi: 10.1021/pr070247w; pmid: 17696520

ACKNOWLEDGMENTS

The authors thank members of the Lancaster lab for helpful feedback and discussions, particularly A. Philips and I. Kelava for technical and intellectual input. We also thank the Light Microscopy and NMR facilities of the MRC Laboratory of Molecular Biology, and P. Pritchett and T. Stevens for help with bioinformatics. **Funding:** This work was supported by the Medical Research Council (MC_UP_1201/9) and the European Research Council (ERC STG 757710). **Author contributions:** L.P. designed and conducted experiments, analyzed data, and wrote the manuscript. C.B. performed NMR experiments and analyzed data. J.C. performed electron microscopy and analyzed data. F.B. performed mass spectrometry and analyzed data. M.S. planned and analyzed mass spectrometry. M.A.L. designed and supervised the project, analyzed data, and wrote the manuscript. **Competing interests:** The authors have filed a patent based on the ChP organoid method. **Data and materials availability:** scRNA-seq data are available at chporg.cells.ucsc.edu and on NCBI GEO (GSE150903). All other data are available in the main text or the supplementary materials. H9, H1, and IMR90-4 cells are available from WiCell under a material transfer agreement with WiCell.

SUPPLEMENTARY MATERIALS

science.sciencemag.org/content/369/6500/eaaz5626/suppl/DC1
Materials and Methods
Figs. S1 to S13
Tables S1 to S5
References (*50*–*128*)
MDAR Reproducibility Checklist
Data S1 to S3

View/request a protocol for this paper from *Bio-protocol*.

19 September 2019; accepted 22 May 2020
Published online 11 June 2020
10.1126/science.aaz5626